VIII CONGRESSO NACIONAL DE ENGENHARIA MECÂNICA
UBERLÂNDIA - MG - BRASIL 10 A 15 DE AGOSTO DE 2014

EXPERIMENTAL VALIDATION AND ANALYSIS OF A FINITE ELEMENT MODEL FOR CANTILEVER BEAMS USED IN ATOMIC FORCE MICROSCOPES

Kleber dos Santos Rodrigues, ksrodrigues@usp.br[1]
Marcelo Areias Trindade, trindade@usp.sc.br[1]

[1]São Carlos School of Engineering, University of São Paulo, Av. Trabalhador São Carlense, 400, 13566-590, São Carlos SP, Brazil

Abstract: *Atomic force microscopy (AFM) is one of the most important tools in scanning probe microscopy. It is based on the oscillations of a cantilever beam which interacts with the measured sample. Due to the inherent nonlinearities of the interactions between beam tip and sample, the mathematical modeling of the cantilever beam dynamics has become indispensable to provide a better understanding of its behavior and more robust control design to improve its operation performance. In the present work, the AFM cantilever beam is represented by a sliding-free Bernoulli-Euler beam with a tip mass in its free end. In the sliding base, two models of excitation are considered: imposed force and prescribed displacement. For validation purposes, images obtained in a scanning electron microscope (SEM) were used to estimate the geometric parameters of two different cantilever beams. Using these parameters together with a developed finite element model, the first resonant frequencies of the beams were numerically evaluated and compared to the corresponding values obtained from experimental AFM tunning. With the validated models, the dynamics of the cantilever beams when subjected to tip-sample interactions are analyzed. For the tip-sample interactions, an attraction-repulsion model based on Lennard Jones potential is considered. The numerically obtained responses of the cantilever beams are analyzed using Fast Fourier Transform, phase portraits and time history. In particular, the effect of the nonlinearity of the tip-sample interactions on the dynamical response is analyzed. Finally, comparisons between the two excitation models, imposed force and prescribed displacement, are performed to help understanding which model is the most appropriate.*
keywords*Atomic Force Microscopy, Sliding-free beams, Lennard Jones, finite element method, nonlinear dynamics*

1. INTRODUCTION

The atomic force microscope (AFM) is a device that uses a sharp tip at the free end of a cantilever beam ($\sim 140nm$) to trace the topography of nanoscale samples (Schitter *et al.*, 2004). An important AFM mode of operation is the intermittent (tapping) mode, in which a piezoceramic actuator excites the sliding base of a cantilever beam at or near its resonance frequency. A vibration amplitude of the sliding base is set by the AFM operator while a laser beam detects the cantilever tip deflection. Than, the error between the reference and acquired signals is minimized by a feedback controller. The feedback height correction generates a colored pixel corresponding to the height of the sample surface at this xy coordinate. The nonlinear interactions of the cantilever tip and sample is an important aspect of the AFM operation. Due to this nonlinearities, neither the photodetector nor the control system work efficiently, therefore, the modeling and understanding of the cantilever dynamics is essential to improve the AFM operation (Jalili and Laxminarayana, 2004).

In the last decades, several works were published focusing on the nonlinear dynamics of AFM cantilever beams (Dankowicz, 2006; Misra *et al.*, 2008; Nozaki *et al.*, 2010; Balthazar *et al.*, 2012; Zhao and Dankowicz, 2006). Most of these works use one degree of freedom models to represents the cantilever beam (spring-mass-damper) and, in general, the tip-sample interactions are modeled using Van der Waals theory, Lennard Jones (LJ) potential or the Dejarguin-Muller-Toporov model. One of the disadvantages of these previous approaches is that parametric design is not allowed.

In the present work, two finite element models are proposed for an AFM cantilever beam (with prescribed displacement or imposed force at the sliding base), Using known material and geometrical parameters obtained via Scanning Electron Microscope (SEM) of the cantilever beam, its frequency response function (FRF) is evaluated with both models and compared to experimental FRF obtained through AFM tunning. Then, the validated model is used to simulate the dynamics of the cantilever beam in presence of a sample surface. The cantilever tip-sample interaction forces are modeled using LJ potential.

2. FINITE ELEMENT MODELING

Standard Bernoulli-Euler beam finite element model is considered for the cantilever beam. The beam is considered to be homogeneous and uniform with length L, width b, thickness h and made of a material with Young's modulus E,

Poisson's ratio ν and mass density ρ. As shown in Fig. 1, a concentrated inertia, with mass m_t and moment of inertia I_t, is included at the free end (tip) of the beam.

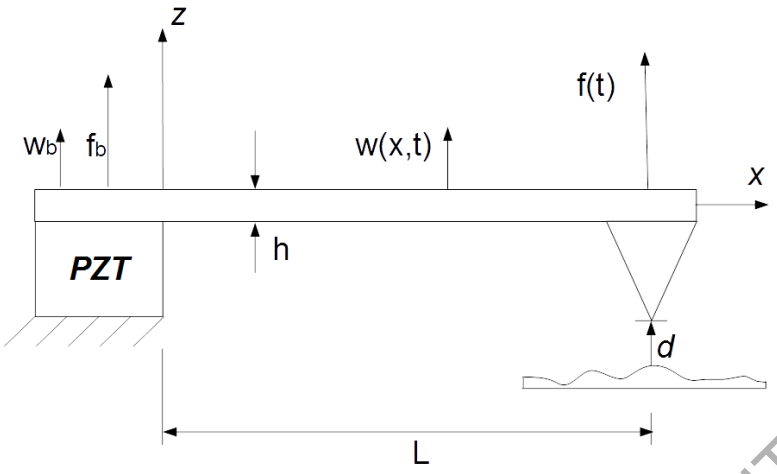

Figure 1: Schematic representation of the AFM cantilever beam.

2.1 Finite element discretization of displacements and strains

Considering the standard Bernoulli-Euler theory for a slender beam in xz plane deflection, the displacements field can be written as

$$\overline{u}(x,y,z,t) = -zw'(x,t),\ \overline{v}(x,y,z,t) = 0,\ \overline{w}(x,y,z,t) = w(x,t), \tag{1}$$

where $w' = \partial w/\partial x$ is the cross-section rotation angle.

Based on these kinematic hypotheses, the only non-null mechanical strain, that is the normal longitudinal strain ε_x, can be written from the usual strain-displacement relation as

$$\varepsilon_x = -zw''. \tag{2}$$

Hermite cubic shape functions are assumed for the discretization of the transverse deflection $w(x,t)$, along the element length L_e, such that a two node finite element with two degrees of freedom per node, namely deflection w_i and cross-section rotation angle w'_i $(i = 1,2)$, is obtained as shown in Fig. 2.

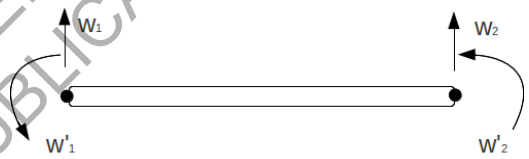

Figure 2: Bernoulli-Euler beam finite element.

The elementary degrees of freedom (dof) column vector $\mathbf{u}_e$ is defined as

$$\mathbf{u}_e = \begin{bmatrix} w_1 \\ w'_1 \\ w_2 \\ w'_2 \end{bmatrix}. \tag{3}$$

2.2 Equations of motion for the AFM cantilever beam accounting for the probe tip

The variational equation of motion of the cantilever beam may be written as:

$$\delta\Pi = \int \left\{ \delta\mathbf{u}^{\mathrm{t}} (\mathbf{M}\ddot{\mathbf{u}} + \mathbf{D}\dot{\mathbf{u}} + \mathbf{K}\mathbf{u} - \mathbf{F}) + \left[\delta w(L,t) m_t \ddot{w}(L,t) + \delta w'(L,t) I_t \ddot{w}'(L,t) \right] \right\} \mathrm{d}t = 0, \tag{4}$$

where $\mathbf{u}$ is the global dof vector, $\mathbf{M}$, $\mathbf{D}$ and $\mathbf{K}$ are global mass, damping and stiffness matrices and $\mathbf{F}$ is the global applied forces vector. Notice that both the deflection and cross-section rotation angle at the beam tip, $w(L,t)$ and $w'(L,t)$, are included in the global dof vector $\mathbf{u}$ and, thus,

$$w(L,t) = \mathbf{L}_w \mathbf{u},\ w'(L,t) = \mathbf{L}_{wx} \mathbf{u}, \tag{5}$$

with

$$\mathbf{L}_w = \begin{bmatrix} 0 & \cdots & 0 & 1 & 0 \end{bmatrix},\ \mathbf{L}_{wx} = \begin{bmatrix} 0 & \cdots & 0 & 1 \end{bmatrix}. \tag{6}$$

Replacing (5) in (4) leads to

$$(\mathbf{M} + \mathbf{M}_t)\ddot{\mathbf{u}} + \mathbf{D}\dot{\mathbf{u}} + \mathbf{K}\mathbf{u} = \mathbf{F}, \tag{7}$$

where the equivalent mass matrix corresponding to the probe tip, $\mathbf{M}_t$, is written as

$$\mathbf{M}_t = \mathbf{L}_w^{\mathrm{t}} m_t \mathbf{L}_w + \mathbf{L}_{wx}^{\mathrm{t}} I_t \mathbf{L}_{wx}. \tag{8}$$

The ad-hoc damping matrix **D** included in the equations of motion was considered to be proportional to the cantilever beam mass and stiffness matrices, **M** and **K**, such that

$$\mathbf{D} = \alpha \mathbf{M} + \beta \mathbf{K}, \tag{9}$$

where the constants α and β must be determined a posteriori. A modal reduction was performed in the system and can be found, as well as more details on the finite element model, in (Rodrigues and Trindade, 2013).

3. BOUNDARY CONDITIONS

Tip-sample interaction forces are implemented as force boundary conditions at the free end of the cantilever beam ($x = L$). For the base excitation, two methods are considered: prescribed displacement and imposed force at the sliding base ($x = 0$).

3.1 Interactions forces between probe tip and sample surface

In the present work, a non-smooth LJ potential model is considered to represent the interactions between the cantilever tip and sample surface. LJ potential describes the interactions between two uncharged molecules or atoms. The diagram in Fig. 3 is a representation of how atoms in probe tip and sample interact, the greater the distance, the less interaction (Salvadori, 2013).

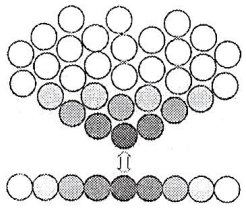

Figure 3: Scheme of molecular interaction (Salvadori, 2013).

According to Rutzel *et al.* (2003), it is reasonable to use LJ potential in AFM, since it represents both long range attractive and short range repulsive forces, present in the tip-sample system.

Considering a probe tip with radius R and a function $r(t)$ that represents the distance between probe tip and sample, the LJ potential energy function $P_{LJ}(r)$ and corresponding interaction force $F_{LJ}(r)$ may be written as (Israelachvli, 1991; Rutzel *et al.*, 2003):

$$P_{LJ}(r) = \frac{H_1 R}{1260 r(t)^7} - \frac{H_2 R}{6 r(t)} \tag{10}$$

and

$$F_{LJ}(r) = \frac{\partial P_{LJ}}{\partial r(t)} = \frac{H_1 R}{180 r(t)^8} - \frac{H_2 R}{6 r(t)^2}. \tag{11}$$

where H_1 and H_2 are the Hamaker constants for the attractive and repulsive potentials. They may be written as $H_1 = \pi^2 C_1 \rho_1 \rho_2$ and $H_2 = \pi^2 C_2 \rho_1 \rho_2$, where ρ_1 and ρ_2 are the number of atoms per unit volume in the each body and C_1 and C_2

are the interaction coefficients of particle-particle intermolecular potential (Rutzel *et al.*, 2003). Therefore, for a known probe tip, the Hamaker constant may vary depending on the material properties of the sample surface (Israelachvli, 1991).

Considering its dynamic variation, due to the cantilever beam deflection, the distance between probe tip and sample surface is written as

$$r(t) = d + w(L,t), \tag{12}$$

where d is the non deflected tip-sample distance, and $w(L,t)$ is the deflection of the cantilever beam tip. In a region very close to the surface, the regions with attractive and repulsive regimes have to be differentiated. Assuming that a_0 is the repulsive region, in a distance larger than a_0 only the attractive term of LJ potential will be considered. In a distance smaller than a_0 the interaction between repulsive and attractive forces is considered. According to Stark *et al.* (2004) and Babahosseini *et al.* (2009), the distance a_0 is approximately $3\mathring{A}$.

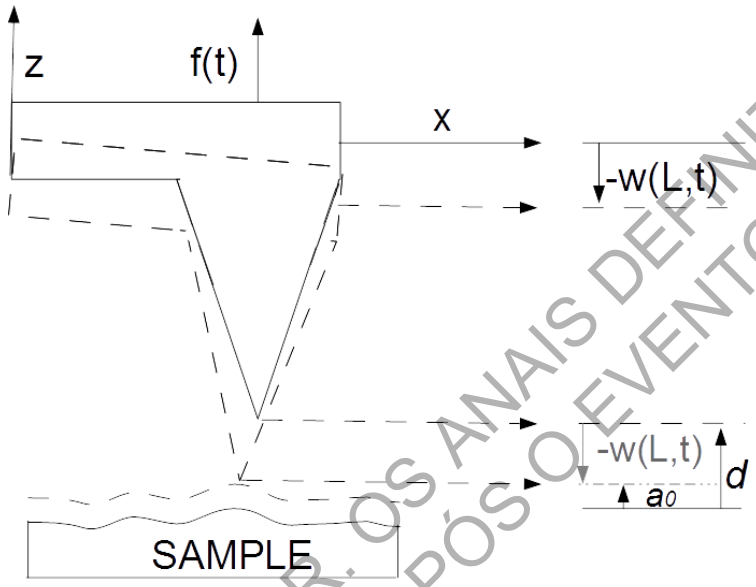

Figure 4: Scheme of cantilever deflection.

Considering Fig. 4 and replacing Eq. (12) in Eq. (11), the force element $f_t(t)$ may be written as

$$f_t(t) = \begin{cases} -\dfrac{H_2 R}{6r(t)^2}, & \text{if } r(t) > a_0 \\ \dfrac{H_1 R}{180 r(t)^8} - \dfrac{H_2 R}{6r(t)^2}, & \text{if } 0 < r(t) \leq a_0 \end{cases} \tag{13}$$

In order to include (13) into the finite element model, a force vector $\mathbf{F}_t(t) = \mathbf{b}_t f_t(t)$ is defined, where $\mathbf{b}_t = [0 \cdots 0\ 1\ 0]$ is a boolean vector that associates the force amplitude $f_t(t)$ with the nodal dof corresponding to the transverse displacement at the free end of the microcantilever beam. This force vector is then included as an applied mechanical forces vector in equation Eq. (7).

3.2 Base excitation of AFM microcantilever beam

Considering only the transversal displacement in $x = 0$, with the beam cross-section rotation angle set to zero ($w'(0,t) = 0$), two different approaches were used to account for the transversal excitation: either an imposed force $f_b(t)$ applied to the moving base of the cantilever beam or a prescribed displacement $w(0,t) = w_b(t)$ of the moving base.

In the case of imposed transversal force, a force vector $\mathbf{F}_b(t) = \mathbf{b}_b f_b(t)$ is defined, where $\mathbf{b}_b = [1\ 0 \cdots\ 0]$ is a boolean vector that associates the force amplitude $f_b(t)$ with the nodal dof corresponding to the transverse displacement at the base of the microcantilever beam (Rodrigues and Trindade, 2013). A known sinusoidal excitation force is considered, such that $f_b(t) = \tilde{f}_b \sin(\omega_{bi} t)$.

In the case of prescribed displacement, the finite element model degree of freedom corresponding to the transversal displacement at the moving base is separated from the others, so that the equations of motion Eq. (7) are rewritten as

$$\begin{bmatrix} \delta w_b & \delta \mathbf{u}_r^{\mathrm{t}} \end{bmatrix} \left\{ \begin{bmatrix} M_{pp} & \mathbf{M}_{pr} \\ \mathbf{M}_{pr}^{\mathrm{t}} & \mathbf{M}_{rr} \end{bmatrix} \begin{bmatrix} \ddot{w}_b \\ \ddot{\mathbf{u}}_r \end{bmatrix} + \begin{bmatrix} D_{pp} & \mathbf{D}_{pr} \\ \mathbf{D}_{pr}^{\mathrm{t}} & \mathbf{D}_{rr} \end{bmatrix} \begin{bmatrix} \dot{w}_b \\ \dot{\mathbf{u}}_r \end{bmatrix} + \begin{bmatrix} K_{pp} & \mathbf{K}_{pr} \\ \mathbf{K}_{pr}^{\mathrm{t}} & \mathbf{K}_{rr} \end{bmatrix} \begin{bmatrix} w_b \\ \mathbf{u}_r \end{bmatrix} - \begin{bmatrix} f_p \\ \mathbf{F}_r \end{bmatrix} \right\} = 0, \tag{14}$$

where $w_b(t)$ is the prescribed displacement at the base of the cantilever beam and $\mathbf{u}_r$ is the remaining unknown dofs vector. Then, considering that $\delta w_b = 0$, since w_b is prescribed, the first line of Eq. (14) is automatically satisfied and the terms involving w_b can be included as an equivalent force applied to the remaining system

$$\mathbf{M}_{rr}\ddot{\mathbf{u}}_r + \mathbf{D}_{rr}\dot{\mathbf{u}}_r + \mathbf{K}_{rr}\mathbf{u}_r = \mathbf{F}_r + \mathbf{F}_b, \tag{15}$$

where the equivalent force vector $\mathbf{F}_p$ associated with the prescribed base displacement is written as

$$\mathbf{F}_b = -(\mathbf{M}^{\mathrm{t}}_{pr}\ddot{w}_b + \mathbf{D}^{\mathrm{t}}_{pr}\dot{w}_b + \mathbf{K}^{\mathrm{t}}_{pr}w_b) \tag{16}$$

If a known sinusoidal base transversal displacement is considered, such that $w_b(t) = \tilde{w}_b \sin(\omega_b t)$, the corresponding force vector $\mathbf{F}_b$ is

$$\mathbf{F}_b = -[(-\omega_b^2\mathbf{M}^{\mathrm{t}}_{pr} + \mathbf{K}^{\mathrm{t}}_{pr})\sin(\omega_b t) + \omega_b\mathbf{D}^{\mathrm{t}}_{pr}\cos(\omega_{bp}t)]\tilde{w}_b. \tag{17}$$

4. MODEL VALIDATION AND NONLINEAR ANALYSIS RESULTS

The goal of this section is to validate the mathematical model through comparison between experimental data and numerical results.

4.1 Model Validation

The experimental data was acquired via SEM and AFM at the Thin Films Laboratory (LFF) in the Physics Institute of the University of São Paulo (IFUSP). The cantilever tip was modeled as a cone, thereby, tip mass and inertia moment were estimated and are shown in Table 1. The figures 5(a) and 5(b) present the images obtained for a cantilever beam using SEM.

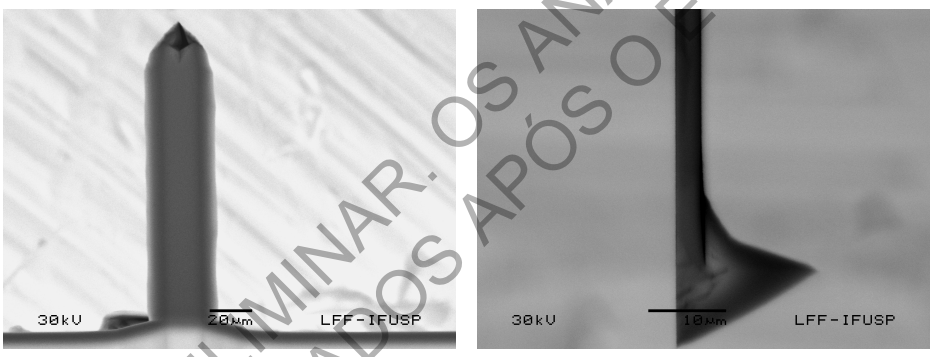

(a) Cantilever frontal view (b) Cantilever side view

Figure 5: Cantilever images

Table 1: Known material parameters and estimated geometrical parameters based on SEM images for an AFM cantilever.

Parameter	**Symbol**	**Value**	**Unit**
Length of microcantilever	L	140	μm
Width of the microcantilever	b	33	μm
Thickness of the microcantilever	h	3.37	μm
Young Modulus	E	176×10^9	N/m^2
Microcantilever density	ρ	2330	Kg/m^3
Second moment of area	I	105.25	μm^4
Area	A	111.21	μm^2
Tip radius	R	150	nm
Tip mass	m_t	3×10^{-10}	Kg
Tip moment of inertia	I_t	23.4×10^{-22}	Kgm^2

Considering the parameters presented in Table 1 and the cantilever beam with free tip (that is, without tip-sample interaction forces), the FRFs for both models were evaluated and compared to experimental ones obtained using AFM tunning. Results are shown in Fig. 6. They were also used to evaluate the resonance frequency of the cantilever beam.

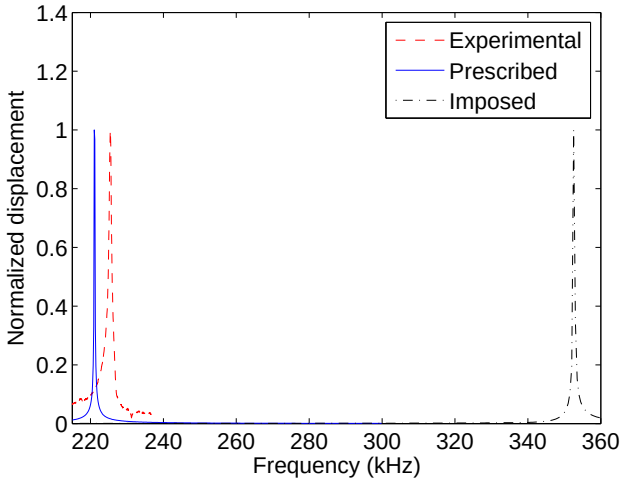

Figure 6: Comparison between experimental data and numerical simulations, red: experimental data, blue: Prescribed displacement, black: imposed force.

Table 2 presents the resonance peak frequencies for both models and relative errors compared to the experimental value.

Table 2: Experimental and numerical peak frequencies (*kHz*)

	Peak	**Relative Error**
Experimental	225.65	–
Prescribed displacement model	220.65	2%
Imposed force model	352.5	56.21%

It is concluded that the model with prescribed displacement presents better results and, thus, will be considered for future simulations.

Fig 7 shows the FRFs zoomed near the resonance frequency. In this preliminary study, this comparison was only used to validate the finite element model, but it could and will also be used to estimate damping properties to be included in the model.

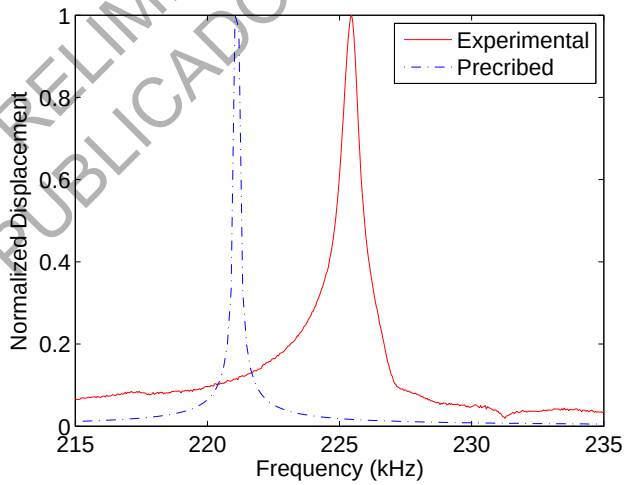

Figure 7: Comparison between prescribed displacement model and experimental data

Based on satisfactory results obtained by prescribed displacement model, it is now used for a nonlinear analysis of the dynamics of the cantilever beam when subjected to tip-sample interaction forces.

4.2 Nonlinear analysis results

The simulations were performed in order to compare the system with and without the tip-sample interactions (relying on LJ potential). Using an harmonic excitation with prescribed displacement, a time response analysis was performed via Fast Fourier Transform (Fft), time history and phase portrait. A proportional damping was considered with $\alpha = \beta = 10^{-6}$, and the parameters of the tip-sample interactions model are shown in Table 3.

Table 3: Parameters

Parameter	**Symbol**	**Value**	**Unit**
Repulsive Hammaker constant	H_1	1.3956×10^{-16}	Jnm^6
Attractive Hammaker constant	H_2	865×10^{-19}	J
Excitation Frequency Prescribed Displacement	ω_{bp}	210.9×10^3	Hz
Tip-sample distance	d	40	nm
Presc. displacement amplitude	$\tilde{w}_b$	30	nm

Results in figure 8(a) shown that the system free of LJ potential presents a predominant peak in the excitation frequency with a small variation at its resonance one. On the other hand the system with LJ potential (Fig. 8(b)) presents several peaks in different frequencies, evidencing the presence of nonlinearities when the tip-sample interactions were considered.

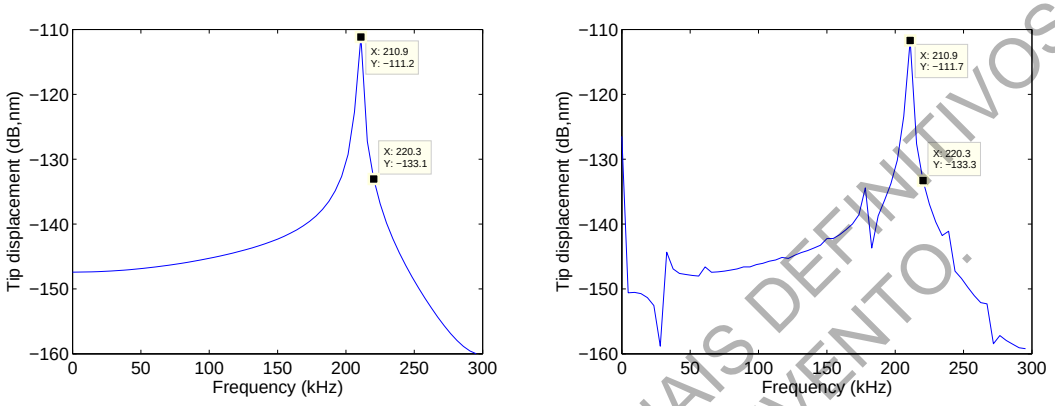

(a) Without LJ potential (b) With LJ potential

Figure 8: Comparison between the system with and without LJ potential

In time history results, the system free of LJ potential has a regular and symmetrical tip displacement amplitude. Without LJ potential, its also features regular motion. Due to the action of repulsive forces, the symmetry disappears flattening the vibration amplitude, when tip approaches the sample surface.

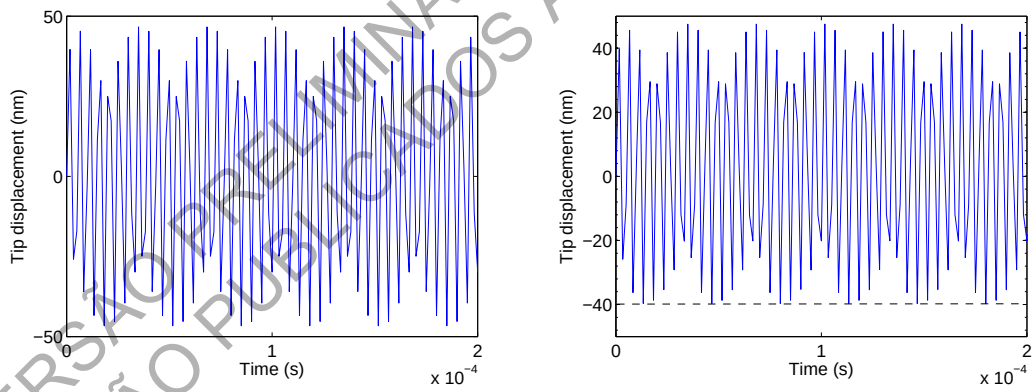

(a) Without LJ potential (b) With LJ potential

Figure 9: Comparison between the system with and without LJ potential

As we can see from Fig 10(a), the points have a symmetry around the origin in the phase portrait of the system without LJ potential, which is a typical feature of linear systems. On the other hand, the system with LJ potential, in Fig 10(b), shows a decrease of velocity and a flattening of the displacement in the region close to the sample surface.

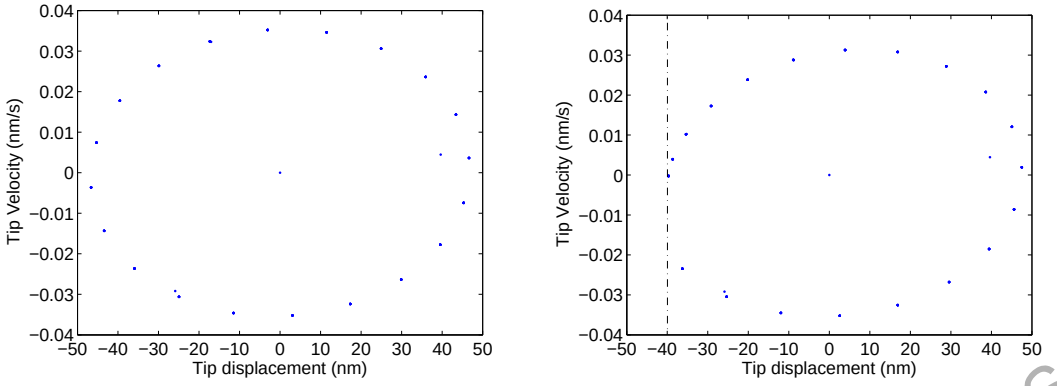

(a) Without LJ potential (b) With LJ potential

Figure 10: Comparison between the system with and without LJ potential

5. CONCLUSIONS

The goal of this work was to validate the finite element model proposed by Rodrigues and Trindade (2013) using known geometrical parameters and resonance peak value obtained by experimental data. The validation of both models, with imposed force and prescribed displacement were performed and the comparison with the experimental data showed different results. While the imposed model showed a peak resonance much larger than the experimental data ($> 50\%$), the model with prescribed displacement showed satisfactory result, with a peak frequency 2% smaller than the experimental one. Therefore, the model with prescribed displacement was selected for future numerical simulations.

The simulations were performed in order to understand the influence of the tip-sample interactions (LJ potential). Therefore, the simulations were performed with and without the influence of LJ potential. Without LJ potential, the cantilever tip displacement was symmetrical and the fft showed only the presence of the excitation frequency. With LJ potential, the cantilever tip displacement was asymmetrical, which showed the presence of a repulsive region, flattening the tip displacement amplitude. The fft analysis showed a large number of resonance peaks and the phase portrait showed decrease of velocity and flattening of tip displacement, result of the nonlinear tip sample interactions, . Thereby, it is concluded that with known geometrical parameters, the prescribed displacement cantilever beam finite element model proposed, showed to be feasible and may be used for future works, which could consider the presence of a sample thin water film, a damping analysis, as well as different models of tip-sample interactions.

6. ACKNOWLEDGEMENTS

Support of MCT/CNPq/FAPEMIG National Institute of Science and Technology on Smart Structures in Engineering, grant 574001/2008-5, is acknowledged. The first author acknowledges also the support of CAPES for a doctoral scholarship. The use of the SPM facility (FAPESP grant $95/5651-0$) of the IFUSP Thin Film Laboratory (LFF/IFUSP/USP) is acknowledged.

7. REFERENCES

Babahosseini, H., Meghdari, A., Khorsand, M. and Alasty, A., 2009. "Optimal sliding mode control of AFM tip vibration and position during manipulation of a nanoscape". In *Proceedings of the ASME 2009 International Mechanical Engineering Congress and Exposition*. pp. 1–10.

Balthazar, J.M., Tusset, A.M. and Bueno, A.M., 2012. "On control strategies, including parametric errors, applied to an Atomic Force Microscope nonlinear vibrating problem". In *1st International Symposium on Uncertainty Quantification and Stochastic Modeling (Uncertainties 2012)*. Maresias, SP.

Dankowicz, H., 2006. "Nonlinear dynamics as an essential tool for non-destructive characterization of soft nanostructures using tapping-mode atomic force microscopy." *Philosophical transactions. Series A, Mathematical, physical, and engineering sciences*, Vol. 364, No. 1849, pp. 3505–20.

Israelachvli, J.N., 1991. *Intermolecular and Surface Forces*. Academic Press, 2nd edition.

Jalili, N. and Laxminarayana, K., 2004. "A review of atomic force microscopy imaging systems: application to molecular metrology and biological sciences". *Mechatronics*, Vol. 14, No. 8, pp. 907–945.

Misra, S., Dankowicz, H. and Paul, M.R., 2008. "Event-driven feedback tracking and control of tapping-mode atomic force microscopy". *Proceedings of the Royal Society A: Mathematical, Physical and Engineering Sciences*, Vol. 464, No. 2096, pp. 2113–2133.

Nozaki, R., Balthazar, J.M. and Tusset, A.M., 2010. "Optimal linear control to an atomic force microscope (afm) problem with chaotic behavior". In *Proceedings of 9th Brazilian Conference of Dynamics and Their Applications (DINCON)*. Serra Negra, SP, pp. 371–377.

Rodrigues, S. and Trindade, M.A., 2013. "Modeling a simulation of a vibrating microcantilever beam in atomic force

microscopes". *Proceedings of 22nd ABCM International Congress of Mechanical Enginnering (COBEM), Ribeirão Preto, SP*.

Rutzel, S., Lee, S.I. and Raman, A., 2003. "Nonlinear dynamics of atomic-force-microscope probes driven in Lennard-Jones potentials". *Proceedings of the Royal Society A: Mathematical, Physical and Engineering Sciences*, Vol. 459, No. 2036, pp. 1925–1948.

Salvadori, C., 2013. "Lecture notes: Scanning tunneling and atomic force microscope". *Thin Film Lab, Phisics Institute, Usp*.

Schitter, G., Allgöwer, F. and Stemmer, a., 2004. "A new control strategy for high-speed atomic force microscopy". *Nanotechnology*, Vol. 15, No. 1, pp. 108–114.

Stark, R., Schitter, G., Stark, M., Guckenberger, R. and Stemmer, A., 2004. "State-space model of freely vibrating and surface-coupled cantilever dynamics in atomic force microscopy". *Physical Review B*, Vol. 69, No. 8, pp. 1–9.

Zhao, X. and Dankowicz, H., 2006. "Characterization of intermittent contact in tapping-mode atomic force microscopy". *Journal of Computational and Nonlinear Dynamics*, Vol. 1, No. 2, pp. 109–115.

8. RESPONSIBILITY NOTICE

The authors are the only responsible for the printed material included in this paper.